JOURNAL OF GUIDANCE, CONTROL, AND DYNAMICS
Vol. 32, No. 6, November–December 2009

Spaceborne Autonomous Relative Control System for Dual Satellite Formations

Jean-Sébastien Ardaens* and Simone D'Amico†
DLR, German Aerospace Research Center, 82230 Wessling, Germany

DOI: 10.2514/1.42855

Autonomous formation flight is a technical challenge of great interest for many scientific missions. Among other applications, the design of synthetic apertures is a promising benefit of using distributed spacecraft. Even if numerous studies exist in the literature, the formation flying concepts and applications were until now rather theoretical. The TanDEM-X Autonomous Formation Flying system presented in this paper will be implemented in the upcoming TanDEM-X mission and contributes as such to increase the readiness level of this technology. The paper focuses on the design of a guidance, navigation, and control system enabling the autonomous relative control of two spacecraft flying on near-circular orbits. Emphasis is given to the practical implementation within an onboard embedded computer, which requires a simple, resource-sparing, and robust design of the system. Therefore, the algorithms are tailored to minimize the usage of onboard resources and to allow the harmonious integration of the relative control system within the space segment. The validation of TanDEM-X Autonomous Formation Flying performed using a hardware-in-the-loop testbed shows that control performance at the meter level is expected.

Nomenclature

a	=	semimajor axis
B	=	ballistic coefficient
e	=	eccentricity
$\boldsymbol{e}_N$	=	unit vector in normal direction
$\boldsymbol{e}_R$	=	unit vector in radial direction
$\boldsymbol{e}_T$	=	unit vector in along-track direction
i	=	inclination
J_2	=	geopotential second-order zonal coefficient
$\boldsymbol{K}$	=	Kalman gain
M	=	mean anomaly
n	=	mean orbit motion
$R_\oplus$	=	equatorial radius of the Earth
$\boldsymbol{r}$	=	inertial position
$\boldsymbol{r}_{\mathrm{EF}}$	=	Earth-fixed position
T	=	control period
t	=	time
u	=	mean argument of latitude
$\boldsymbol{v}_{\mathrm{EF}}$	=	Earth-fixed velocity
$\boldsymbol{v}$	=	inertial velocity
Δa	=	relative semimajor axis
$\Delta \boldsymbol{e}$	=	relative eccentricity vector
$\Delta \boldsymbol{i}$	=	relative inclination vector
Δu	=	relative mean argument of latitude
$\Delta \boldsymbol{r}$	=	relative position
$\Delta \boldsymbol{\alpha}$	=	relative orbit elements
$\Delta \boldsymbol{v}$	=	relative velocity with respect to Hill's comoving frame
δi_T	=	variation of Δi_y over one control period
$\delta \Delta u_d$	=	variation of Δu over one control period due to the drag
$\delta \Delta u_{J2}$	=	variation of Δu over one control period due to J_2
$\delta \Delta u_{\Delta V}$	=	variation of Δu over half an orbit period caused by a maneuver
δe	=	size of the relative eccentricity vector
δi	=	size of the relative inclination vector
$\delta \varphi_T$	=	phase variation of $\Delta \boldsymbol{e}$ over one control period
ε	=	size of the tolerance window
θ	=	phase of the relative inclination vector
μ	=	Earth's gravitational parameter
ρ	=	atmospheric density
φ	=	phase of the relative eccentricity vector
Ω	=	right ascension of the ascending node
ω	=	argument of perigee
$\omega_\oplus$	=	Earth-angular velocity

I. Introduction

FORMATION flying is one of the most promising technologies for future space missions. The distribution of sensors and payloads among several spacecraft allows higher redundancy, flexibility, and new applications that would not be possible with a single spacecraft. Among others, one may mention the design of virtual telescopes at a libration point [1], a laser interferometer for the detection of gravitational waves [2], or an interferometric synthetic aperture radar (SAR) for Earth observation [3]. However, the high scientific gain potentially afforded by these new missions comes at the expense of a higher system complexity and costs. As a consequence, few ideas have been already concretized even if theoretical studies about formation flying abound.

The first formation flying missions to make use of a set of satellites to achieve a scientific goal were Earth observation missions. They belong to a class of missions for which the technical difficulties are usually well known and, thus, are natural candidates to gain the necessary experience in designing and operating formations of satellites. The Gravity Recovery and Climate Experiment (GRACE), composed of two low-Earth-orbit satellites flying on the same orbit with a separation of 200 ± 50 km, has already demonstrated the successful use of a ground-in-the-loop controlled formation for scientific purposes [4]. Future missions will, however, most likely use autonomously controlled formations that reduce the need for ground station visibility. In addition, autonomy provides better control performances, reactivity in case of contingency, and a reduction in the ground support and costs.

This paper presents a complete guidance, navigation, and control (GNC) architecture able to enable the autonomous relative control of a generic low-Earth mission composed of two satellites equipped

Received 20 December 2008; revision received 13 July 2009; accepted for publication 13 July 2009.

*Scientist, Global Navigation Satellite System Technology and Navigation Group, German Space Operations Center.

†Scientist, Global Navigation Satellite System Technology and Navigation Group, German Space Operations Center.

with Global Navigation Satellite System (GNSS) sensors and flying on near-circular orbits with typical separations of several hundred meters. The focus is given to the design of a simple and functional system to be embedded in a spacecraft platform and able to fulfill the control requirements, ensure the safety of the formation, minimize the usage of onboard resources, and satisfy the operational constraints. The backbone of the system is an innovative parameterization of the relative motion in terms of relative orbit elements on which the formation design as well as the navigation, guidance, and control algorithms are based [5]. This parameterization is used in the analytical model of the relative motion, in the definition of the state of the formation, in the assessment of the collision risk, and in the design of guidance rules and control feedback laws. The choice of a unified parameterization throughout the complete GNC system ensures an inherent consistency and simplicity during the development of algorithms.

The modeling and parameterization of the relative motion of coorbiting satellites in a formation has been extensively investigated in the past. The Clohessy–Wiltshire (CW) relative equations of motion [6] were derived in 1960 to simulate rendezvous operations and used a Hill-like [7] rotating Cartesian coordinate frame with the origin on the leader satellite to express the relative state vector of a chaser satellite. The linear formulation of these equations assumes small deviations from a circular reference orbit about a spherical Earth; they can be integrated to provide a time-explicit analytical solution. Many authors have worked to generalize these equations to include disturbance forces [8,9] and eccentric reference orbits [10,11].

The simplicity of the CW model makes it well suited for real-time onboard applications with limited computational resources. However, its classical Cartesian description does not provide a straightforward interpretation of the geometry of the relative motion. The analytical solution of the linear CW equations comprises six integration constants that depend on the initial relative state. Many efforts have been made to express them in a convenient way, by introducing relative orbit elements that offer the possibility of describing the geometry of the relative trajectory [5,12,13]. The use of relative orbit elements was found to be extremely useful when trying to minimize the collision hazard of colocated satellites placed on geostationary orbits. In fact, a proper selection of the relative orbit elements guarantees a minimum spatial separation of the satellites [14]. The parameterization used throughout this paper is derived from this idea. Together with a simple extended CW dynamical model that includes the perturbation caused by the Earth's oblateness, it offers a simple and powerful mathematical tool to predict the relative motion and assess the risk of collision. The efficiency of this parameterization was first successfully demonstrated during the swap of the GRACE satellites [15]. The TanDEM-X mission, composed of two satellites flying in close formation, has been designed using the same parameterization to ensure a passive safety of the formation [16]. More recently, the modeling of perturbations affecting this relative motion model was refined within the framework of the PRISMA mission [17].

The controller is designed using a simple impulsive relative control strategy. This choice is preferable for missions for which a continuous thrust is not advisable [18], which is often the case for Earth observation missions. In addition, the resulting closed-form analytical solution offers the advantage of simplicity for the onboard algorithms and transparency for the mission operations and planning, because the size and the location of maneuvers are predictable. Gauss's variational equations of motion are well suited to the impulsive control design [19,20]. They provide a direct relationship between the orbit elements and the control action and, until now, have been used intensively for absolute station keeping. Strong interest arises now to exploit them for relative orbit control of formation described by means of the relative orbit elements [21,22]. In addition, some authors have already demonstrated the power of Gauss's variational equations applied to a relative control problem in the presence of the Earth's oblateness effect [21–24]. The parameterized relative motion model adopted throughout the paper has the advantage of being easily invertible to yield directly the solution of Gauss's variational equations for the retained set of relative orbit elements. These equations provide a straightforward relation between a spacecraft velocity increment and the resulting variation of the relative orbit elements of the formation. They have also been used for the relative orbit control design of the PRISMA formation flying demonstration mission [17].

The relative control system presented in the paper will be used in the TanDEM-X mission to enable the autonomous in-plane relative control of the formation. The TanDEM-X mission is composed of two satellites flying in close formation, which will be operated as a flexible SAR interferometer. Its primary goal is the generation of a global digital elevation model of the Earth's surface with unprecedented accuracy [3]. The first satellite, called TSX, was launched in June 2007 and is currently operating as a repeat-pass interferometer within the framework of the TerraSAR-X mission. It will be supplemented in the second half of 2009 by the second satellite, called TDX. Together, both satellites will build a single pass interferometer that is no longer affected by the decorrelation of SAR signals and will thus improve the quality of the scientific products.

Short and flexible baselines between the satellites are required to build the virtual SAR interferometer. The typical distances are between several hundred meters and a few kilometers. To that end, the formation has been designed to obtain a passively safe natural elliptic relative motion [16]. To reduce the secular drift of the relative inclination vector, the inclination of the TSX and TDX orbits has been chosen to be identical. TSX is the leader of the formation, which has to follow a reference trajectory, whereas TDX is the chaser, which has to replicate all the absolute maneuvers done by TSX. In addition, TDX will perform small corrections to maintain the formation using a dedicated cold gas propulsion system comprising two branches of four 40 mN thrusters.

The formation acquisition and reconfiguration will be performed by the ground segment. Even if the formation keeping requirements can be fulfilled by a ground-in-the-loop control scheme, it has been recognized that the current technologies are mature enough to allow the implementation of an embedded autonomous relative control system, called TanDEM-X Autonomous Formation Flying (TAFF). TAFF promises many benefits. It will ease the ground support and demonstrate the resulting reduction of costs. It will also improve the control performances and, thus, the quality of the data products and help provide experience in using and operating an autonomously controlled formation. For simplicity, TAFF will replace only the relative in-plane control of the formation. The out-of-plane relative motion does not require frequent corrections (one maneuver every month) and will be thus controlled by the ground segment. The system requirements state that the TAFF system shall provide an orbit control accuracy in an along-track direction of 200 m (1σ) for along-track separations of 5 km and perpendicular to the flight direction of $1/15$th (1σ) of the radial/cross-track separations.

Robustness, simplicity, and the limited usage of onboard resources are the main design drivers for TAFF. To that end, an analytical solution of the impulsive control problem using the retained parameterization of the relative motion has been derived to implement the control algorithms. The controller is fed by an optimized observer that computes the set of relative orbit elements from onboard GNSS navigation sensors. Both satellites are equipped with single-frequency MosaicGNSS [25] GPS receivers providing a real-time filtered navigation solution sampled at 1 Hz. The TSX navigation data are transmitted via an S-band intersatellite link that can work at a distance of up to 4 km. A synchronized set of navigation solutions is provided every 10 s to TAFF.

Emphasis has been given to the functional and performance validation of the system. In particular, it has to be ensured that the system is able to fulfill the relative control requirements while coping with the operational constraints and the limitations imposed by the available onboard resources. For this purpose, a hardware-in-the-loop testbed has been set up. It comprises a realistic simulation environment running on a host computer and including an accurate modeling of the perturbations acting on low-Earth-orbiting spacecraft, of the sensors and actuators, and of the basic interactions with the ground segment. The GNC flight software is running on a target computer representative of the onboard computer in a real-time

environment. The expected system performance and software resource usage are presented in Sec. III.B.

II. Relative Control System Design

A. System Definition and Requirements

The relative control system presented in the paper applies to a class of formations composed of two satellites flying on near-circular orbits with small separations of several hundred meters to a few kilometers. Furthermore, it is assumed that the formation is designed to make use of the orbit dynamics to obtain a natural elliptic relative motion. To that end, two nearly identical orbits with identical semimajor axes but slightly different eccentricities, inclinations, arguments of perigee, and ascending nodes are chosen. Such a formation configuration is, for example, of interest for SAR interferometry missions because it allows small and naturally time-dependent separations between the spacecraft [3]. The relative control system is required to be easy to operate, robust, and resource saving with control performance at the meter level. The focus is given to the autonomous onboard control of the formation, called relative control. The formation acquisition and reconfiguration is supposed to be done by the ground segment. Any change in the orbit of the formation, called absolute control in the sequel, is also controlled on ground. In this case, both satellites need to execute the same maneuver to keep the shape of the formation unchanged. A distinction is made between the leader satellite, which serves as a reference for the formation and may need to follow a user-defined trajectory, and the chaser satellite, which has to maintain a relative trajectory with respect to the leader. The relative control system is located on the chaser. Its objective consists of keeping the formation as close as possible to a nominal configuration. The leader is passive in the adopted formation control scheme. Both satellites are equipped with GNSS positioning sensors that provide real-time three-dimensional absolute position and velocity information in an Earth-fixed reference frame. An intersatellite link is used to exchange data between the spacecraft.

B. Reparameterization of the Clohessy–Wiltshire Model

The Keplerian elements of the chaser and leader orbits (identified, respectively, by the subscripts 1 and 2) are used to define a relative eccentricity vector $\Delta\boldsymbol{e}$ and a relative inclination vector $\Delta\boldsymbol{i}$. With e, i, ω, and Ω denoting, respectively, the eccentricity, inclination, argument of perigee, and right ascension of the ascending node, we introduce

$$\Delta\boldsymbol{e} = e_2\begin{pmatrix}\cos\omega_2\\ \sin\omega_2\end{pmatrix} - e_1\begin{pmatrix}\cos\omega_1\\ \sin\omega_1\end{pmatrix} \tag{1}$$

and

$$\Delta\boldsymbol{i} = \begin{pmatrix} i_2 - i_1 \\ (\Omega_2 - \Omega_1)\sin i_1\end{pmatrix} = \begin{pmatrix}\Delta i \\ \Delta\Omega \sin i_1\end{pmatrix} \tag{2}$$

In the sequel, the relative eccentricity and inclination vectors are described either by their Cartesian or their polar representation using the following notation:

$$\Delta\boldsymbol{e} = \begin{pmatrix}\Delta e_x\\ \Delta e_y\end{pmatrix} = \delta e\begin{pmatrix}\cos\varphi\\ \sin\varphi\end{pmatrix} \quad \text{and} \quad \Delta\boldsymbol{i} = \begin{pmatrix}\Delta i_x\\ \Delta i_y\end{pmatrix} = \delta i\begin{pmatrix}\cos\theta\\ \sin\theta\end{pmatrix} \tag{3}$$

A set of relative orbit elements $\Delta\boldsymbol{\alpha}$ is then defined by introducing the relative semimajor axis $\Delta a = a_2 - a_1$ and the relative mean argument of latitude $\Delta u = u_2 - u_1$:

$$\Delta\boldsymbol{\alpha} = \begin{pmatrix}\Delta a\\ a_1\Delta e_x\\ a_1\Delta e_y\\ a_1\Delta i_x\\ a_1\Delta i_y\\ a_1\Delta u\end{pmatrix} = \begin{pmatrix} a_2 - a_1 \\ a_1(e_2\cos(\omega_2) - e_1\cos(\omega_1)) \\ a_1(e_2\sin(\omega_2) - e_1\sin(\omega_1)) \\ a_1(i_2 - i_1) \\ a_1(\Omega_2 - \Omega_1)\sin(i_1) \\ a_1(u_2 - u_1)\end{pmatrix} \tag{4}$$

where the nondimensional orbit elements have been multiplied by the semimajor axis of the chaser to obtain consistent units among all the components of the vector and to ease the geometrical interpretation. Because the spacecraft are supposed to fly in close formation, the quadratic differences of orbit elements are neglected in the following linearization process. As a consequence, the subscripts of the absolute orbit elements are removed in the sequel. The description of the relative motion of the leader with respect to the chaser is conveniently made in Hill's local comoving frame $(\boldsymbol{e}_R, \boldsymbol{e}_T, \boldsymbol{e}_N)$, with the origin at the center of mass of the chaser. The unit vector $\boldsymbol{e}_R$ is aligned with the radial direction, positive outward, and $\boldsymbol{e}_N$ is aligned with the orbit angular momentum, whereas $\boldsymbol{e}_T$ points in the along-track direction and completes the triad. For any spacecraft with inertial position $\boldsymbol{r}$ and velocity $\boldsymbol{v}$, the three unit vectors are mathematically defined as follows:

$$\boldsymbol{e}_R = \frac{\boldsymbol{r}}{|\boldsymbol{r}|}; \qquad \boldsymbol{e}_N = \frac{\boldsymbol{r}\times\boldsymbol{v}}{|\boldsymbol{r}\times\boldsymbol{v}|}; \qquad \boldsymbol{e}_T = \boldsymbol{e}_N \times \boldsymbol{e}_R \tag{5}$$

The relative position $\Delta\boldsymbol{r} = \boldsymbol{r}_2 - \boldsymbol{r}_1$ mapped within this frame may be written as

$$\Delta\boldsymbol{r} = \Delta r_R\boldsymbol{e}_R + \Delta r_T\boldsymbol{e}_T + \Delta r_N\boldsymbol{e}_N \tag{6}$$

whereas the relative velocity $\Delta\boldsymbol{v}$ with respect to Hill's frame is written as

$$\Delta\boldsymbol{v} = \Delta v_R\boldsymbol{e}_R + \Delta v_T\boldsymbol{e}_T + \Delta v_N\boldsymbol{e}_N \tag{7}$$

It can be shown [15,16] that the solution of the linearized Hill–Clohessy–Wiltshire equations of motion for unperturbed near-circular orbits can be parameterized with the relative orbit elements defined in Eq. (4). The resulting equations provide a direct mapping between the relative position and velocity in Hill's frame at time t and the relative orbit elements taken at the epoch t_0:

$$\begin{pmatrix}\Delta r_R\\ \Delta r_T\\ \Delta r_N\\ \Delta v_R/n\\ \Delta v_T/n\\ \Delta v_N/n\end{pmatrix} = \begin{bmatrix} 1 & -\cos u & -\sin u & 0 & 0 & 0 \\ -\frac{3}{2}(u-u_0) & 2\sin u & -2\cos u & 0 & \cot i & 1 \\ 0 & 0 & 0 & \sin u & -\cos u & 0 \\ 0 & \sin u & -\cos u & 0 & 0 & 0 \\ -3/2 & 2\cos u & 2\sin u & 0 & 0 & 0 \\ 0 & 0 & 0 & \cos u & \sin u & 0\end{bmatrix}\Delta\boldsymbol{\alpha} \tag{8}$$

where u and u_0 stand, respectively, for the mean argument of latitude at time t and t_0. The mean motion n used in the equation is defined as

$$n = \sqrt{\mu/a^3} \tag{9}$$

where μ is the Earth's gravitational parameter. Equation (8) shows clearly that a bounded relative motion can only be achieved if $\Delta a = 0$. As a consequence, any formation must fulfill this condition to be stable. Furthermore, the in-plane motion, that is, the motion in the $(\boldsymbol{e}_R, \boldsymbol{e}_T)$ plane, is a centered ellipse only if the relative mean argument of latitude is chosen as

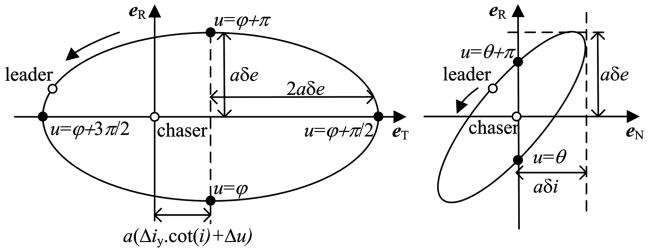

Fig. 1 Projection of the relative motion of the leader with respect to the chaser for any configuration with $\Delta a = 0$: a) along-track/radial plane, and b) cross-track/radial plane.

$$\Delta u = -\cot i \cdot \Delta i_y \tag{10}$$

As depicted in Fig. 1 the use of relative orbit elements gives an immediate overview of the geometry of the relative motion. Whereas the size of the in-plane elliptic motion is driven by $a\delta e$, the out-of-plane motion depends on $a\delta i$. The quantities Δa and Δu shift the in-plane ellipse in the radial and tangential directions, respectively.

Furthermore, Eq. (8) shows that a proper phasing of $\Delta\boldsymbol{e}$ and $\Delta\boldsymbol{i}$ ($\Delta\boldsymbol{e}$ parallel to $\Delta\boldsymbol{i}$) ensures that the cross-track separation is maximal when the radial separation vanishes, and vice versa. In this case, the minimal separation in the plane perpendicular to the flight direction equals the minimum of $(a\delta i, a\delta e)$. Because of the fact that $\Delta\boldsymbol{e}$ and $\Delta\boldsymbol{i}$ evolve relatively slowly over time (c.f. Sec. II.C), the relative motion in the $(\boldsymbol{e}_R, \boldsymbol{e}_N)$ plane is stable and easily predicable. On the contrary, any uncertainty or small change of the value Δa will result in a drift of Δu [cf. Eq. (8)], making it more difficult to predict the along-track component of the relative motion. As a result a proper selection of the relative orbit elements ensures a minimum separation perpendicular to the flight direction and, thus, guarantees that the spacecraft will never collide over a long period. Thus, the adopted parameterization offers a simple criterion, called in the literature the separation of the relative e/i vector [16], to assess the collision risk of the formation and provide a passive safety to the formation.

C. Modeling of Perturbed Relative Motion

The classical Keplerian orbit elements $(a, e, i, \omega, \Omega, M)$ are constant except for the mean anomaly M, for which the time derivative is given by

$$\dot{M} = n \tag{11}$$

Considering that $u = M + \omega$, the time derivative of the relative mean argument of latitude becomes to a first order approximation

$$\Delta\dot{u} = n_2 - n_1 = \sqrt{\mu/a_2^3} - \sqrt{\mu/a_1^3} \approx -\tfrac{3}{2}\sqrt{\mu/a^3}\,\Delta a \tag{12}$$

Because the other relative orbit elements composing $\Delta\boldsymbol{\alpha}$ are a combination of constant classical orbit elements, its time evolution in the case of a Keplerian motion can be easily derived:

$$\Delta\dot{\boldsymbol{\alpha}} = (0 \quad 0 \quad 0 \quad 0 \quad 0 \quad -\tfrac{3}{2}n\Delta a)^T \tag{13}$$

The formation undergoes various perturbations that are not expressed in the simplified dynamics of Eq. (13). The most important contribution is due to the nonuniformity of the Earth's gravity field, which induces periodic and secular perturbations of the orbit elements. In particular, if $R_\oplus$ is the equatorial radius of the Earth, J_2 is the second-order zonal coefficient of the gravity field, and

$$\gamma = \frac{J_2}{2}\left(\frac{R_\oplus}{a(1-e^2)}\right)^2 \tag{14}$$

the secular effect of J_2 on the orbit elements is given by [26]

$$\frac{\mathrm{d}}{\mathrm{d}t}\begin{pmatrix} a \\ e \\ i \\ \omega \\ \Omega \\ u \end{pmatrix} = \frac{\mathrm{d}}{\mathrm{d}t}\begin{pmatrix} a \\ e \\ i \\ \omega \\ \Omega \\ \omega + M \end{pmatrix} = \begin{pmatrix} 0 \\ 0 \\ 0 \\ \tfrac{3}{2}n\gamma(5\cos^2 i - 1) \\ -3n\gamma\cos i \\ \tfrac{3}{2}n\gamma((5\cos^2 i - 1) + \sqrt{1-e^2}(3\cos^2 i - 1)) \end{pmatrix} \tag{15}$$

By substituting Eq. (15) in the time derivative of Eq. (4), one obtains, after neglecting the second-order terms in the orbit elements differences and after some manipulations [5],

$$\Delta\dot{\boldsymbol{\alpha}} = \begin{pmatrix} 0 \\ -\tfrac{3}{2}n\gamma(5\cos^2 i - 1)\cdot a\Delta e_y \\ \tfrac{3}{2}n\gamma(5\cos^2 i - 1)\cdot a\Delta e_x \\ 0 \\ 3n\gamma\sin^2 i \cdot a\Delta i_x \\ -12n\gamma\sin(2i)\cdot a\Delta i_x - \tfrac{3}{2}n\cdot\Delta a \end{pmatrix} \tag{16}$$

According to Eq. (16), $\Delta\boldsymbol{e}$, $\Delta\boldsymbol{i}$, and Δu are altered over the long term. $\Delta\boldsymbol{e}$ rotates with an angular drift rate

$$\dot{\varphi} = \tfrac{3}{2}n\gamma(5\cos^2 i - 1) \tag{17}$$

whereas the y component of $\Delta\boldsymbol{i}$ undergoes a linear drift that depends on the difference in inclination. In the case of a formation flying at a 500 km altitude with an inclination of $i = 98$ deg, the relative eccentricity vector $\Delta\boldsymbol{e}$ makes a complete revolution in about 100 days. As a direct consequence, a safe formation that has been designed using the relative eccentricity/inclination vector concept may become unsafe.

In addition, other perturbations that are difficult to model (e.g., differential drag caused by different ballistic coefficients between the spacecraft) or even unpredictable (e.g., random thruster errors) affect the formation and need to be compensated for. In particular, the maneuver execution errors during absolute orbit corrections are a major source of disturbance for the formation. To keep the formation unchanged, any absolute maneuver done by the leader must be replicated by the chaser. In the presence of random thruster errors for both spacecraft, a differential velocity increment will be induced that tends to alter the geometry of the formation.

D. Guidance and Control Design

The set of relative orbit elements $\Delta\boldsymbol{\alpha}$ used until now to describe and design the formation is also exploited in the control strategy. Considering a formation configuration defined by the nominal set $\Delta\boldsymbol{\alpha}^n$ of relative orbit elements, the relative control of the formation consists of keeping the actual state $\Delta\boldsymbol{\alpha}$ sufficiently close to the nominal configuration at any time:

$$|\Delta\alpha_i - \Delta\alpha_i^n| < \varepsilon_i \quad \forall\ i \tag{18}$$

where the subscript i denotes the ith component of the vectors. A simple guidance approach could consist of letting the relative orbit elements evolve within a tolerance window centered on their nominal values and correcting them to the nominal values as soon as the condition defined by Eq. (18) is violated. Another possibility retained in this paper is to correct them at a regular period T, called control period, small enough to ensure that the drift of the relative elements stays within the tolerance window. This approach strengthens the

determinism and the predictability of the guidance behavior and might be preferable from a mission operation and planning point of view. The control period T is then chosen depending on the desired control accuracy.

In fact, the control of only Δa, $\Delta \boldsymbol{e}$, and $\Delta \boldsymbol{i}$ is enough to fully control the relative motion, because the time derivative of Δu is proportional to Δa. According to Eq. (13), a difference Δa of semimajor axis during a time span δt induces a variation of the relative mean argument of latitude:

$$\delta \Delta u = -\tfrac{3}{2} n \delta t (\Delta a / a) \tag{19}$$

Because the time evolution of the relative eccentricity and inclination vectors can be modeled, it is convenient to derive a simple deterministic guidance law that estimates the drift of $\Delta \boldsymbol{e}$ and $\Delta \boldsymbol{i}$ over one control period and tries to keep the time-averaged values of $\Delta \boldsymbol{e}$ and $\Delta \boldsymbol{i}$ close to the nominal values. In particular, the phase of the relative eccentricity vector $\Delta \boldsymbol{e}$ drifts during the control period by an angle of

$$\delta \varphi_T = \dot{\varphi} \cdot T \tag{20}$$

whereas the y component of $\Delta \boldsymbol{i}$ undergoes, during the same time interval, a linear drift that amounts to

$$\delta i_T = 3 n \gamma \sin^2 i \cdot \Delta i_x \cdot T \tag{21}$$

A control strategy that keeps $\Delta \boldsymbol{e}$ and $\Delta \boldsymbol{i}$ centered on their nominal values and controls them at a period T ensures that the phase φ of $\Delta \boldsymbol{e}$ remains within a tolerance of $\pm \delta \varphi_T / 2$, whereas Δi_y remains within a tolerance of $\pm \delta i_T / 2$ (Fig. 2).

The guidance law is realized by planning a desired value $\Delta \boldsymbol{e}^{\text{man}}$, corresponding to the lower extremity of the tolerance window, at the beginning of the control cycle and letting $\Delta \boldsymbol{e}$ drift over time to achieve the targeted value $\Delta \boldsymbol{e}^t$, corresponding to the upper extremity of the tolerance window, at the end of the control period. The same consideration applies to the desired and targeted values $\Delta \boldsymbol{i}^{\text{man}}$ and $\Delta \boldsymbol{i}^t$. The desired values are simply defined as follows:

$$\Delta \boldsymbol{e}^{\text{man}} = \boldsymbol{R}(-\delta \varphi_T / 2) \Delta \boldsymbol{e}^n \quad \text{and} \quad \Delta \boldsymbol{i}^{\text{man}} = \Delta \boldsymbol{i}^n - \begin{pmatrix} 0 \\ \delta i_T / 2 \end{pmatrix} \tag{22}$$

where $\boldsymbol{R}$ stands for the elementary two-dimensional rotation matrix. This guidance approach requires a correction of the relative orbit elements, which is described in the sequel by the operator $\delta \Delta(.) = \Delta(.)^{\text{man}} - \Delta(.)$. The variation of orbit elements caused by one maneuver executed on the chaser can be easily retrieved by inverting the relative motion model described earlier. The inversion of Eq. (8) yields

$$\Delta \boldsymbol{\alpha} = \begin{pmatrix} 4 & 0 & 0 & 0 & 2 & 0 \\ 3\cos(u) & 0 & 0 & \sin(u) & 2\cos(u) & 0 \\ 3\sin(u) & 0 & 0 & -\cos(u) & 2\sin(u) & 0 \\ 0 & 0 & \sin(u) & 0 & 0 & \cos(u) \\ 0 & 0 & -\cos(u) & 0 & 0 & \sin(u) \\ 6(u-u_0) & 1 & \cos(u)\cot(i) & -2 & 3(u-u_0) & -\sin(u)\cot(i) \end{pmatrix} \begin{pmatrix} \Delta r_R \\ \Delta r_T \\ \Delta r_N \\ \Delta v_R / n \\ \Delta v_T / n \\ \Delta v_N / n \end{pmatrix} \tag{23}$$

If we set $\Delta r_R = \Delta r_V = \Delta r_N = 0$ and $u = u_0$, then Eq. (23) describes the difference in terms of orbit elements between two spacecraft located at the same position but with a different velocity at time $t = t_0$. In other words, the inversion of the linear relative motion model provides the direct relation between an instantaneous velocity increment in Hill's orbital frame and the consequent change of orbit elements. This simply corresponds to Gauss' variational equations [20], adapted to near-circular orbit and rewritten to use the parameterization adopted in the paper. Two small manipulations are, however, necessary to retrieve the variation $\delta \Delta \boldsymbol{\alpha}$ of the relative orbit elements of the formation at time t caused by an instantaneous velocity increment $\delta \boldsymbol{v}$ executed at time t_0 by the chaser. First, according to the conventions chosen at the beginning of the paper, the relative orbit elements of the formation correspond to the difference in orbit elements of the leader with respect to the chaser. Because formation keeping maneuvers are executed by the chaser, the variation $\delta \Delta \boldsymbol{\alpha}$ is the opposite of the variation of orbit elements of the chaser. Second, the equations obtained by inverting the relative motion model and setting $\Delta \boldsymbol{r} = 0$, $u = u_0$ yield the variation of relative orbit elements right after the execution of the maneuver. To express $\delta \Delta \boldsymbol{\alpha}$ at time $t > t_0$, one has to consider the variation of Δu during t_0 and t induced by the variation of Δa caused by the maneuver at time t_0, which can be easily done using Eq. (13). We finally obtain

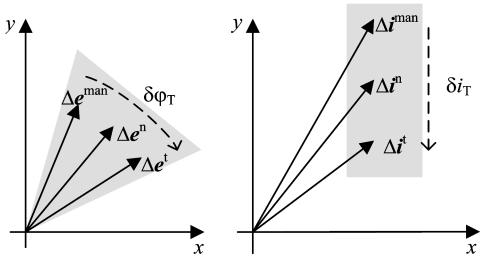

Fig. 2 Tolerance windows (gray areas) around a) the phase of the nominal relative eccentricity vector, and b) the y component of the nominal relative inclination vector.

$$\delta \Delta \boldsymbol{\alpha} = \begin{pmatrix} \delta \Delta a \\ a \delta \Delta e_x \\ a \delta \Delta e_y \\ a \delta \Delta i_x \\ a \delta \Delta i_y \\ a \delta \Delta u \end{pmatrix} = -\frac{1}{n} \begin{bmatrix} 0 & 2 & 0 \\ \sin u & 2\cos u & 0 \\ -\cos u & 2\sin u & 0 \\ 0 & 0 & \cos u \\ 0 & 0 & \sin u \\ -2 & -3n(t-t_M) & -\sin u \cdot \cot(i) \end{bmatrix} \begin{pmatrix} \delta v_R \\ \delta v_T \\ \delta v_N \end{pmatrix} \tag{24}$$

where δv_R, δv_T, and dv_N denote the components of the chaser velocity increment executed at time t_0 written in the aforementioned Hill's frame. Because a cross-track velocity increment affects only $\Delta \boldsymbol{i}$, the control problem can be separated between in-plane relative control, for which a radial and/or tangential control action is used to control Δa, $\Delta \boldsymbol{e}$, and Δu, and out-of-plane control, for which a normal control action is used to control $\Delta \boldsymbol{i}$.

The out-of-plane relative control is the easiest aspect of the impulsive control problem. A desired change $\delta \Delta \boldsymbol{i}$ of the relative inclination vector can be obtained using a single cross-tack maneuver:

$$\delta v_N = -an\|\delta\Delta \boldsymbol{i}\| \quad \text{at } u_M = \arctan\left(\frac{\delta\Delta i_y}{\delta\Delta i_x}\right) \tag{25}$$

Similarly, a desired change $\delta\Delta \boldsymbol{e}$ can be obtained using a single radial maneuver:

$$\delta v_R = -an\|\delta\Delta \boldsymbol{e}\| \quad \text{at } u_M = \pi - \arctan\left(\frac{\delta\Delta e_x}{\delta\Delta e_y}\right) \tag{26}$$

In both cases, an undesired change of Δu is generated during the execution of maneuvers. This can be counteracted by creating a small difference of Δa with an along-track maneuver that will make Δu drift back to its initial value. When using radial maneuvers, the change of Δu can be conveniently counteracted using a double impulse strategy. To that end, the correction is done in two steps so that the offset of Δu induced by the first maneuver is exactly the opposite of the offset induced by the second maneuver. If the two maneuvers are identified by the superscripts 1 and 2, one possible solution is

$$\Delta v_R^1 = -(an/2)\|\delta\Delta \boldsymbol{e}\| \qquad \Delta v_R^2 = +(an/2)\|\delta\Delta \boldsymbol{e}\| \tag{27}$$

at the following mean arguments of latitude:

$$u_{M1} = \pi - \arctan\left(\frac{\delta\Delta e_x}{\delta\Delta e_y}\right) \quad \text{and} \quad u_{M2} = u_1 + \pi \tag{28}$$

The main advantage of the double impulse strategy is that no change of semimajor axis is required to confine Δu within the tolerance window. However, Δa, which undergoes the perturbation of the drag, and Δu, which undergoes the perturbation due to J_2 and of the drag, still need to be actively controlled. The control of Δa is, thus, always required and can only be done using an along-track maneuver [cf. Eq. (24)]. To reduce the complexity of the control strategy, it might be of interest to look for a control scheme that controls $\Delta \boldsymbol{e}$ and Δa at the same time. In fact, a pair of along-track maneuvers is sufficient to obtain a desired correction $\delta\Delta a$ and $\delta\Delta \boldsymbol{e}$:

$$\Delta v_T^1 = -\frac{an}{4}\left(\|\delta\Delta \boldsymbol{e}\| + \frac{\delta\Delta a}{a}\right) \qquad \Delta v_T^2 = +\frac{an}{4}\left(\|\delta\Delta \boldsymbol{e}\| - \frac{\delta\Delta a}{a}\right) \tag{29}$$

at the following mean arguments of latitude:

$$u_{M1} = \arctan\left(\frac{\delta\Delta e_y}{\delta\Delta e_x}\right) \quad \text{and} \quad u_{M2} = u_1 + \pi \tag{30}$$

In addition, Eqs. (27) and (29) show clearly that this solution presents the benefit of being 2 times less expensive in term of fuel consumption when compared with a pair of radial maneuvers. Such an approach requires, however, some care in the computation of the desired relative semimajor axis after the pair of maneuvers. The double impulse solution induces a nonvanishing semimajor axis difference during the two maneuvers that makes the spacecraft drift from each other. The relative control strategy needs to counteract this variation of Δu by targeting a slightly nonzero Δa at the end of the pair of maneuvers, which will make the spacecraft drift back to the other side of the tolerance window (Fig. 3). Here again a predictable and deterministic approach can be adopted to keep the variation of Δu in a tolerance window centered on its nominal value.

A fixed control period T ensures that the variation of $\Delta \boldsymbol{e}$ due to J_2 over one control cycle is always identical and, thus, that the maneuvers are always executed at the same orbit location [cf. Eq. (28)]. As a consequence, it is convenient to parameterize the control period T by an integer number N of orbit revolutions:

$$T = (2\pi/n)N \tag{31}$$

To design the control law it is supposed that the control process is in a stationary mode. In this case, the initial relative semimajor Δa is

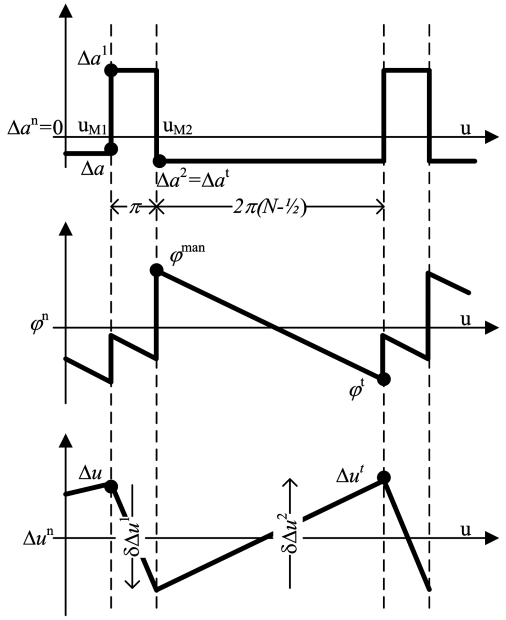

Fig. 3 Variations during a complete control period of a) relative semimajor axis, b) phase of relative eccentricity vector, and c) relative mean argument of latitude.

close to the nominal value $\Delta a^n = 0$, and φ differs from the nominal φ^n by an angle of $\delta\varphi_T/2$. The major variation of relative mean argument of latitude is caused by the difference in semimajor axis induced by the first maneuver during half an orbit, which amounts to [cf. Eq. (13)]

$$a\delta\Delta u_{\Delta v} = -\tfrac{3}{2}\pi\Delta a^1 \tag{32}$$

Considering that the variation of semimajor axis caused by the first maneuver amounts to

$$-\frac{2\delta v_T^1}{n} = \Delta a^1 - \Delta a \approx \Delta a^1 \tag{33}$$

Using Eq. (24) and (29), this becomes

$$\begin{aligned} a\delta\Delta u_{\Delta v} &\approx -\frac{3}{2}\pi\frac{2\delta v_T^1}{n} = -\frac{3\pi}{4}a\left(\|\Delta \boldsymbol{e}^{\text{man}} - \Delta \boldsymbol{e}^t\| + \frac{\delta\Delta a}{a}\right) \\ &\approx \frac{3\pi}{4}\delta\varphi\|a\Delta \boldsymbol{e}^n\| \end{aligned} \tag{34}$$

where it is supposed that the quantity $\Delta a^t - \Delta a \approx 0$ is small compared with the size of $\delta\Delta \boldsymbol{e}$. Over one control period T, the relative mean argument of latitude undergoes the perturbation due to J_2, which amounts to [cf. Eq. (16)]

$$a\delta\Delta u_{J2} = -12n\gamma\sin(2i)\cdot a\Delta i_x \cdot T \tag{35}$$

and the effect of the differential drag, which can be modeled as

$$a\delta\Delta u_d = \tfrac{1}{4}\rho v^2(B_2 - B_1)T^2 \tag{36}$$

where ρ is the atmospheric density, v the spacecraft velocity with respect to the atmosphere, and B_i the spacecraft ballistic coefficients. The latter contribution is, however, small compared with $\delta\Delta u_{\Delta V}$ and $\delta\Delta u_{J2}$ if the spacecraft are similar. For a formation flying at a 500 km altitude with $i_1 = 98$ deg, $i_2 - i_1 = 0.001$ deg, and $a\delta e = 300$ m and controlled every $T = 5$ orbit revolutions, one obtains $a\delta\Delta u_{\Delta V} =$ 14 m and $\delta\Delta u_{J2} = 5.8$ m. Assuming that $\rho = 0.1195$ g/km^3, $v = 7500$ m/s, and that the spacecraft are nearly identical with a difference of 2% in the nominal ballistic coefficient, and taking

$B = 0.0056\ \mathrm{m}^2/\mathrm{kg}$, the offset of $a\Delta u$ induced by the differential drag amounts to only 24 cm. It addition, the computation $a\delta\Delta u_d$ requires the implementation of an atmospheric density model. As a consequence, it might be neglected when trying to optimize the usage of computational resources if the spacecraft are nearly identical. During a control period, the drift of Δu amounts to

$$\delta\Delta u_T = \delta\Delta u_{\Delta v} + \delta\Delta u_{J2} + \delta\Delta u_d \approx \delta\Delta u_{\Delta v} + \delta\Delta u_{J2} \tag{37}$$

A variation of Δu almost centered on its nominal value Δu^n is subsequently achieved by setting a slightly nonzero Δa^t at the end of the pair of maneuvers (cf. Fig. 3) so that the satellites drift to reach, at the end of the control period, the targeted value Δu^t defined as

$$\Delta u^t = \Delta u^n - \delta\Delta u_T/2 \tag{38}$$

Let t_1 denote the time of the execution of the first maneuver and $t_2 = t_1 + \pi/n$ the time of the second maneuver. The first maneuver brings the relative semimajor axis to a new value Δa^1 until the epoch of the second maneuver because the differential drag is neglected. The second maneuver results in the final value Δa^t (i.e., the target relative semimajor axis at the end of the pair of maneuvers) for the relative semimajor axis until $t_3 = t_1 + T$, the time of the next control sequence.

The total variation of Δu over the control period is (cf. Fig. 3)

$$\delta\Delta u = \Delta u^t - \Delta u = \delta\Delta u^1 + \delta\Delta u^2 \tag{39}$$

where $\delta\Delta u^1$ is the variation of the relative mean argument of latitude introduced by Δa^1 during π/n, and $\delta\Delta u^2$ is the one introduced by Δa^2 during $T - \pi/n$. Equation (19) yields

$$\begin{cases} \delta\Delta u^1 = -\frac{3}{2}\pi(\Delta a^1/a) \\ \delta\Delta u^2 = -\frac{3}{2}n(T - (\pi/n))(\Delta a^2/a) = -3\pi(N - \frac{1}{2})(\Delta a^t/a) \end{cases} \tag{40}$$

Using Eqs. (24) and (29), we can formulate the variation of the relative semimajor axis introduced by the two maneuvers $\delta\Delta a^1 = \Delta a^1 - \Delta a$ and $\delta\Delta a^2 = \Delta a^2 - \Delta a^1$ in function of the desired relative semimajor axis Δa^t at the end of the pair of maneuvers

$$\begin{cases} \delta\Delta a^1 = \Delta a^1 - \Delta a = -(2/n)\Delta v_T^1 = +(a/2)(\|\delta\Delta \boldsymbol{e}\| + (\delta\Delta a/a)) \\ \delta\Delta a^2 = \Delta a^2 - \Delta a^1 = -(2/n)\Delta v_T^2 = -(a/2)(\|\delta\Delta \boldsymbol{e}\| - (\delta\Delta a/a)) \end{cases} \tag{41}$$

Using Eqs. (39–41), one obtains

$$\begin{aligned} \Delta u^t - \Delta u = \delta\Delta u^1 + \delta\Delta u^2 = -(3\pi/a)((3\Delta a/4) \\ - (a/4)\|\delta\Delta \boldsymbol{e}\| + (N - (3/4))\Delta a^t) \end{aligned} \tag{42}$$

Finally, the target relative semimajor axis after the pair of maneuvers is

$$\Delta a^t = \left(-\frac{(\Delta u^t - \Delta u)a}{3\pi} - \frac{\Delta a}{4} - \frac{a\|\delta\Delta \boldsymbol{e}\|}{4}\right) \cdot \frac{1}{N - \frac{1}{4}} \tag{43}$$

In a real-time implementation, it is not advisable to compute the size of the two maneuvers in advance, because the execution error of the first maneuver may have some influence on the size of the second one. Thus, it is preferable to plan the first one using Eq. (29). Right after the execution of the first maneuver, the relative semimajor axis has reached the value Δa^1. Because its location is already chosen, the only purpose of the second maneuver is to bring back Δa to the initially targeted value Δa^T computed in Eq. (43). This can be simply achieved using Eq. (24):

$$\Delta v_T^2 = -(n/2)(\Delta a^T - \Delta a) \tag{44}$$

where Δa is the current relative semimajor axis, that is, right before the execution of the second maneuver. Ideally, Δa amounts to Δa^1 so that the size of the second maneuver computed in real time is the same as the size given by Eq. (29). If not, the real-time implementation will compensate the errors introduced by the first maneuver to reach more precisely the targeted Δa^T after the pair of maneuvers.

E. Observer Design

The guidance and control laws require the accurate knowledge of the relative orbit elements of the formation. In fact, Eq. (19) shows that an error of 5 m in the knowledge of the relative semimajor axis of a formation flying at 500 km altitude results after 1 orbit in a 47 m control error of the relative mean argument of latitude. The GNSS sensors provide in real time the absolute positions and velocities of the spacecraft but with insufficient accuracy, making mandatory the usage of an onboard real-time dynamical filter. In addition, the use of a dynamical model allows the relative navigation filter to cope with possible data gaps of the intersatellite link or with short failures of the sensors. Several approaches are possible to design a filter. Among them, the processing of GNSS raw measurements using a highly accurate dynamical model of the relative motion provides accurate estimations of the relative orbit elements but is complex and computationally intensive. On the contrary, the observer presented in this paper focuses on the simplicity and rapidity of execution. A dynamical filtering of the relative orbit elements is done using a discrete extended Kalman filter (EKF) [27].

An initial a priori value $\Delta\boldsymbol{\alpha}_0$ of the filter state vector is computed from Eq. (23) at time t_0. The input vector $[\Delta r_R \Delta r_T \Delta r_N \Delta v_R/n \Delta v_T/n\Delta v_N/n]^T$ for Eq. (23) is computed using the Earth-fixed position $\boldsymbol{r}_{\mathrm{EF}}$ and velocity $\boldsymbol{v}_{\mathrm{EF}}$ as provided by the spacecraft GNSS receivers. First, Hill's frame $(\boldsymbol{e}_R, \boldsymbol{e}_T, \boldsymbol{e}_N)$ is defined following Eq. (5), which requires the inertial velocity $\boldsymbol{v}$ of the chaser. The inertial velocity $\boldsymbol{v}$ mapped in the Earth-fixed frame can be defined from the Earth-fixed velocity $\boldsymbol{v}_{\mathrm{EF}}$ using

$$\boldsymbol{v} = \boldsymbol{v}_{\mathrm{EF}} + (\,0 \quad 0 \quad \omega_\oplus\,)^T \times \boldsymbol{r}_{\mathrm{EF}} \tag{45}$$

where $\omega_\oplus$ stands for the angular velocity of the Earth. The relative velocity $\Delta\boldsymbol{v}$ (leader with respect to the chaser in Hill's frame) mapped in the Earth-fixed frame is computed using the relative position $\Delta\boldsymbol{r}_{\mathrm{EF}}$ and the relative Earth-fixed velocity $\Delta\boldsymbol{v}_{\mathrm{EF}}$:

$$\Delta\boldsymbol{v} = \Delta\boldsymbol{v}_{\mathrm{EF}} + (\,0 \quad 0 \quad \omega_\oplus\,)^T \times \Delta\boldsymbol{r}_{\mathrm{EF}} - n\boldsymbol{e}_N \times \Delta\boldsymbol{r}_{\mathrm{EF}} \tag{46}$$

Finally, $\Delta\boldsymbol{r}$ and $\Delta\boldsymbol{v}$ are mapped to Hill's frame to provide the input vector of Eq. (23). The current mean argument of latitude u of the chaser can be retrieved using

$$u = \arctan 2\left(\frac{\boldsymbol{k}\cdot\boldsymbol{r}_{\mathrm{EF}}}{\boldsymbol{j}\cdot\boldsymbol{r}_{\mathrm{EF}}}\right) \tag{47}$$

with

$$\boldsymbol{j} = \frac{\boldsymbol{e}_Z \times \boldsymbol{e}_N}{\|\boldsymbol{e}_Z \times \boldsymbol{e}_N\|}, \qquad \boldsymbol{k} = \boldsymbol{e}_N \times \boldsymbol{j} \tag{48}$$

where $\boldsymbol{e}_Z = (\,0 \quad 0 \quad 1\,)^T$. The time update of the EKF at time t is based on the simple analytical model described by Eq. (16), which does not require any numerical propagation. The drift of $\Delta\boldsymbol{e}$ between two consecutive calls of the EKF is small and simplifies to

$$\Delta\boldsymbol{e} = \begin{pmatrix} \Delta e_x \\ \Delta e_y \end{pmatrix} = \begin{pmatrix} \Delta e_{x0} - \dot{\varphi}(t - t_0)\Delta e_{y0} \\ \Delta e_{y0} + \dot{\varphi}(t - t_0)\Delta e_{x0} \end{pmatrix} \tag{49}$$

where the subscript 0 is employed to describe the values of the previous call. The state transition matrix can be expressed using Eqs. (16) and (49):

$$\boldsymbol{\Phi}(t,t_0)=\left(\frac{\partial\Delta\boldsymbol{\alpha}(t)}{\partial\Delta\boldsymbol{\alpha}(t_0)}\right)=\begin{pmatrix}1&0&0&0&0&0\\0&1&-\dot{\varphi}(t-t_0)&0&0&0\\0&\dot{\varphi}(t-t_0)&1&0&0&0\\0&0&0&1&0&0\\0&0&0&3\gamma\sin^2 i\cdot(u-u_0)&1&0\\-\frac{3}{2}(u-u_0)&0&0&-12\gamma\sin(2i)(u-u_0)&0&1\end{pmatrix} \tag{50}$$

We can take advantage of the sparseness of the state transition matrix to optimize the computation, that is, to avoid useless multiplications, of the updated covariance matrix $\boldsymbol{P}$:

$$\boldsymbol{P}=\boldsymbol{\Phi}\boldsymbol{P}_0\boldsymbol{\Phi}^T+\boldsymbol{Q} \tag{51}$$

where $\boldsymbol{Q}$ stands for the process noise matrix. The process noise matrix is introduced to balance the decrease of covariance when processing new measurements. For simplicity, $\boldsymbol{Q}$ is chosen as diagonal matrix. To ensure optimal filter performance, the proper balance between the process and measurement noise is determined by simulations and will be validated during flight. The execution of any maneuver on the spacecraft is conveniently taken into account using the Gauss variational equations [Eq. (24)] applied to the equivalent impulsive maneuver between t_0 and t. The relative position z obtained by the simple subtraction of the absolute positions mapped in Hill's local frame is used as measurement to perform the measurement update of the EKF. In particular, the modeled observation $\boldsymbol{h}$ is computed from the current state $\Delta\boldsymbol{\alpha}$ using Eq. (8):

$$\boldsymbol{h}=\begin{bmatrix}1&-\cos u&-\sin u&0&0&0\\0&2\sin u&-2\cos u&0&\cot i&1\\0&0&0&\sin u&-\cos u&0\end{bmatrix}\Delta\boldsymbol{\alpha} \tag{52}$$

and the Kalman gain $\boldsymbol{K}$ is computed as

$$\boldsymbol{K}=\frac{\boldsymbol{P}_0\boldsymbol{G}^T}{\sigma^2+\boldsymbol{G}^T(\boldsymbol{P}_0\boldsymbol{G}^T)} \tag{53}$$

where σ is the noise of the measurements and

$$\boldsymbol{G}=\left(\frac{\partial\boldsymbol{h}}{\partial\boldsymbol{X}}\right) \tag{54}$$

The measurement noise is, rigorously speaking, a time-dependent variable because it depends on the geometry of the GPS satellites seen by the receiver. For simplicity, σ is considered as constant and its value is determined from tests conducted with the GPS receiver. Finally, the state vector and the covariance matrix are updated as

$$\Delta\boldsymbol{\alpha}=\Delta\boldsymbol{\alpha}_0+\boldsymbol{K}(z-h)\quad\text{and}\quad\boldsymbol{P}=\boldsymbol{P}_0-\boldsymbol{K}\boldsymbol{G}\boldsymbol{P}_0 \tag{55}$$

It has to be noted that the measurements used by the observer are already filtered navigation solutions from the GNSS receivers. The cascading of filters can be a potential source of instability because it violates Kalman's assumption that the measurements are timewise uncorrelated. However, this issue is not considered to be harmful because the Kalman filter of the GNSS receiver smooths the receiver kinematic fixes over a short time scale, typically 1 min, whereas the Kalman filter of the observer averages the relative orbit elements over a much larger timescale, typically 1 orbit. Tests conducted with the MosaicGNSS receiver do not show any risk of instability.

F. Architectural Design

The complete GNC system is built by combining the observer and controller as presented in the previous sections (cf. Fig. 4). The observer gets as inputs the synchronized GNSS absolute navigation solutions generated on both spacecraft. The dynamically filtered set of relative orbit elements feeds the controller, which implements the guidance and feedback control laws. The time update of the Kalman filter requires a priori information about all the maneuvers executed by the two spacecraft. This includes the autonomously executed formation keeping maneuvers and the maneuvers commanded by the ground segment. Depending on the space segment capabilities, the latter information can be sent via telecommand or retrieved autonomously by the onboard computer and exchanged via the intersatellite link. This option is not always possible but is preferable if a higher level of autonomy is required. A priori autonomous maneuver information is fed back by the controller to the observer.

The knowledge of the relative orbit elements may be conveniently used to provide a real-time analysis of the formation to the attitude and orbit control system (AOCS). The relative state (position and velocity) is retrieved using Eq. (8). The most interesting feature of the adopted parameterization of the relative motion is certainly the ability to estimate the risk of collision by predicting the minimum separation perpendicular to the flight direction between the spacecraft during the next orbits (in the absence of maneuvers) without any resource-consuming numerical propagation. This is possible because the relative orbit elements describe the geometry of

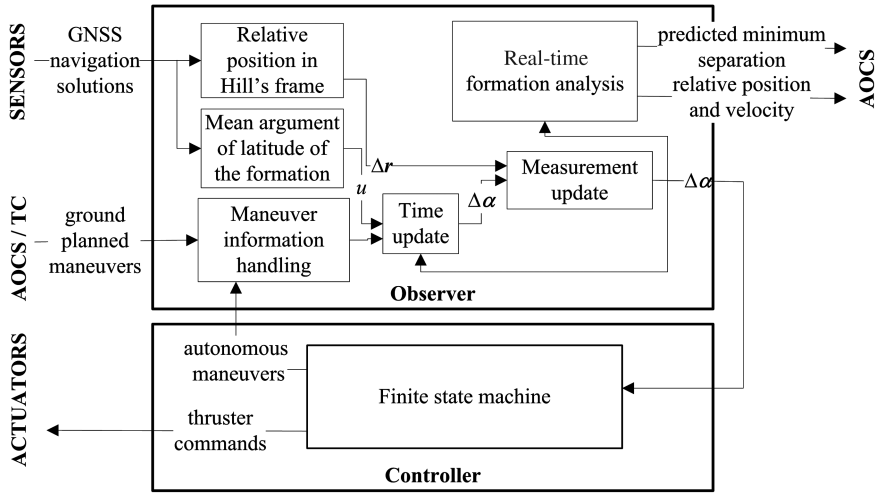

Fig. 4 Simplified architecture of the GNC system.

the elliptic motion. Thus, the minimum separation in the plane $(\boldsymbol{e}_R, \boldsymbol{e}_N)$ can be computed by searching for the minimum of $\Delta r_R^2 + \Delta r_N^2$. Using Eq. (8) and setting $\Delta a = 0$, this minimum amounts to

$$\Delta r_{RN}^{\mathrm{MIN}} = \frac{\sqrt{2} \cdot a \cdot |\Delta \boldsymbol{e} \cdot \Delta \boldsymbol{i}|}{(\delta e^2 + \delta i^2 + \|\Delta \boldsymbol{e} + \Delta \boldsymbol{i}\| \cdot \|\Delta \boldsymbol{e} - \Delta \boldsymbol{i}\|)^{1/2}} \tag{56}$$

To improve the robustness of the control and to ease its monitoring, the control sequence is implemented using a finite state machine depicted in Fig. 5 using the GRAFCET graphical convention [28]. The workflow is defined using a set of states, transitions, and actions. The state machine is updated at a regular frequency. The state (from 0 to 5) is used to store the actual position in the control sequence and may be associated with an action. In this case the action will be performed at every update of the state machine until the state has changed. The switch from the state n to $n + 1$ can be performed only if the state n *is* active and the transition between the state n and $n + 1$ is valid.

III. Case Study: TanDEM-X Autonomous Formation Flying System

A. Description

The GNC algorithms presented in the first part of the paper will be implemented within the framework of the TanDEM-X mission as part of the TDX AOCS. As explained in the Introduction, the TanDEM-X formation is composed of two satellites flying in close formation to build a SAR interferometer. To validate the compliance with the requirements, a sophisticated hardware-in-the-loop simulation is used to ensure realistic assessment of the performance.

B. Performance Assessment

This section focuses on the realistic performance assessment of the relative control system using a hardware-in-the-loop formation flying testbed. It comprises a powerful desktop computer clocked at 2 GHz that simulates the environment as well as the sensors and actuators with a high degree of precision. It comprises also a resource-limited target computer, representative of the onboard computer, on which the flight software is running (cf. Fig. 6).

The absolute motion of the spacecraft is numerically propagated using a 30×30 GGM01S Earth gravity model including the luni–solar perturbations, the atmospheric drag (using the Jacchia–Gill atmospheric density model), the solar radiation pressure (using a cannonball model), and the tidal and relativistic effects. The GNSS sensors are modeled using the Phoenix EMulator (PEM) software, which allows a realistic modeling of the behavior of a Phoenix GPS receiver [29] flying in low Earth orbit. More specifically, it emulates the output messages for raw measurements, navigation solutions, and broadcast ephemerides generated by the Phoenix GPS receiver. In the current simulation only the navigation messages provided by the emulated GPS receivers are used. PEM is tuned to match the characteristics of the MosaicGNSS receiver used on TSX and TDX. Furthermore, the GNSS data coming from the modeled TSX receiver

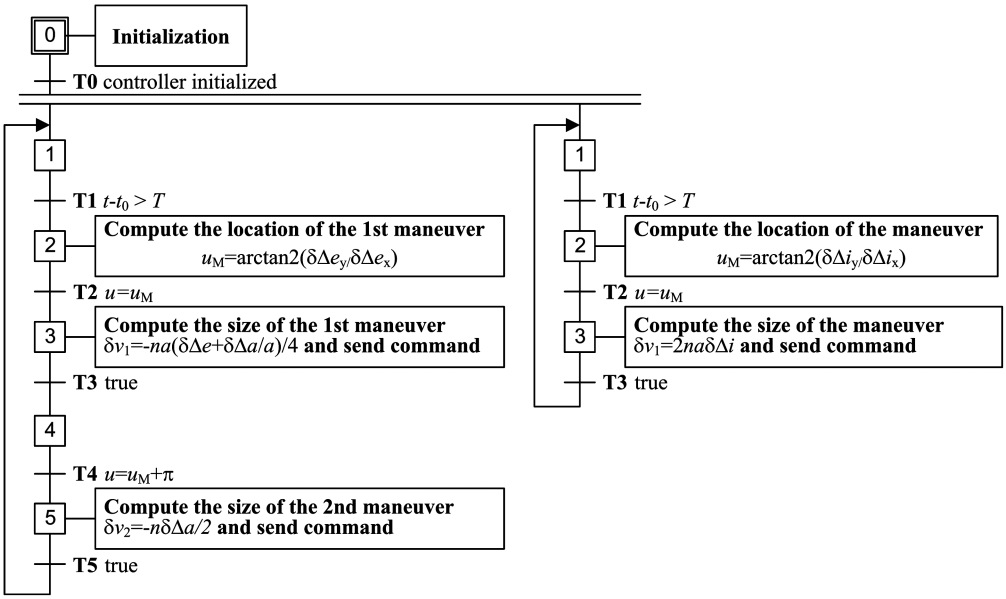

Fig. 5 Graphical representation of the finite state machine governing the in-plane (left) and out-of-plane (right) relative control of the formation.

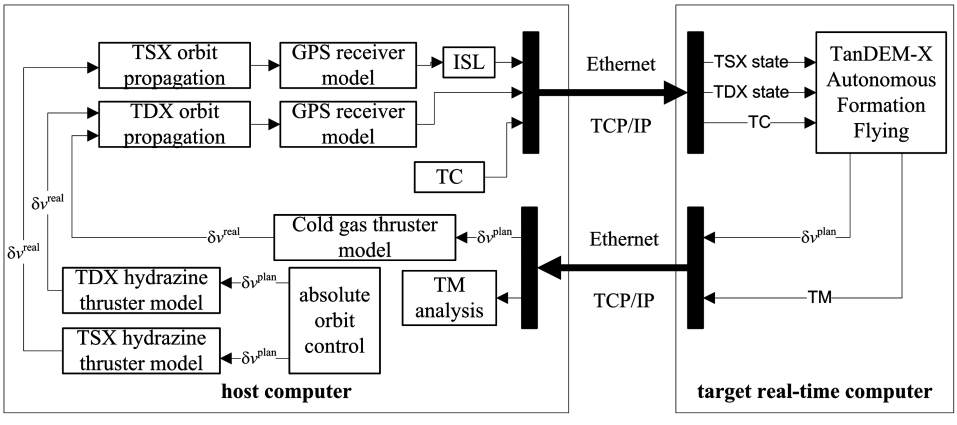

Fig. 6 Simplified architecture of the formation flying testbed used to assess the performances of TAFF.

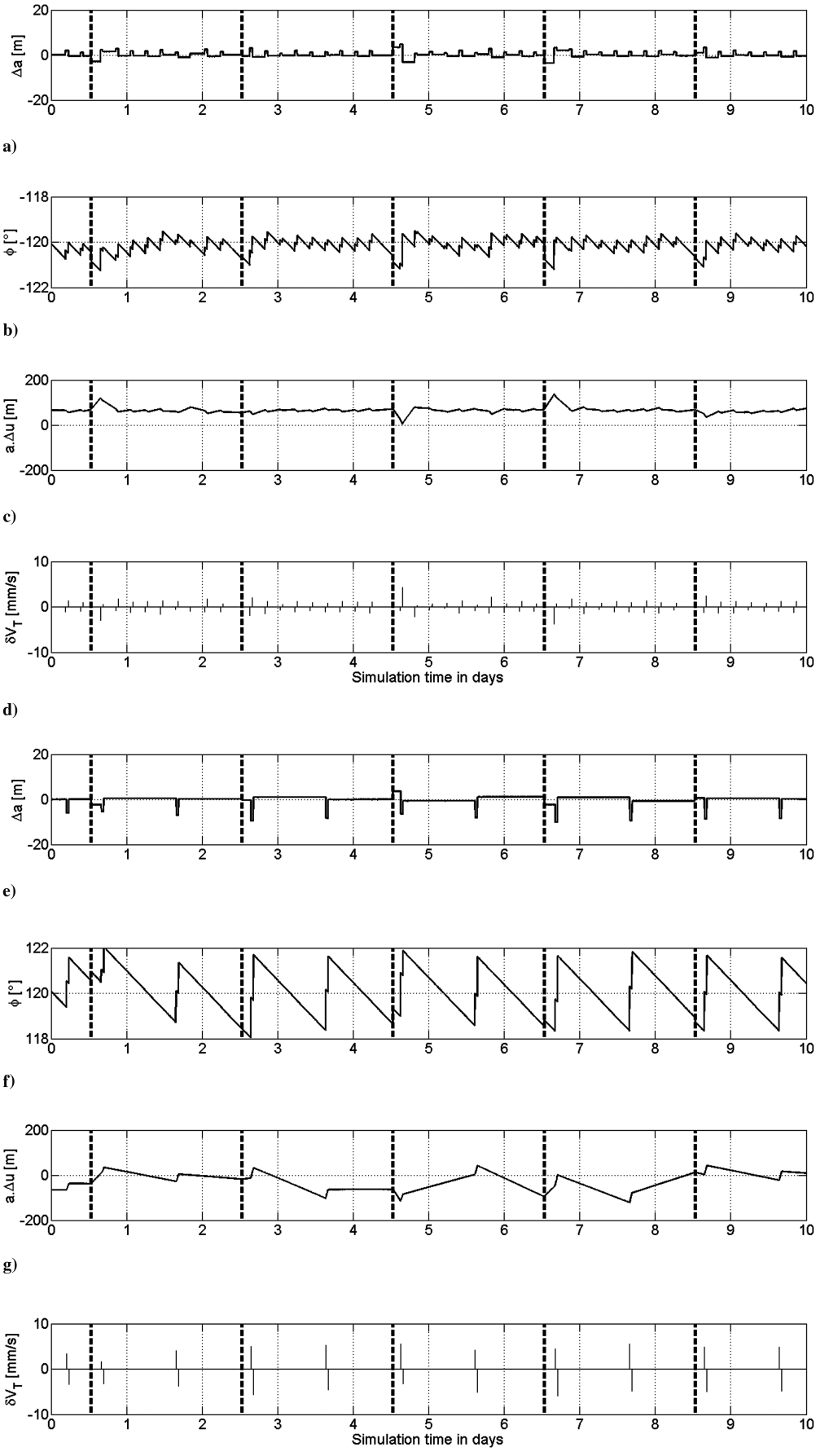

Fig. 7 Control of the formation over 10 days with two different control periods: a, e) relative semimajor axis; b, f) relative argument of perigee; c, g) relative mean argument of latitude; and d, h) tangential maneuvers.

pass through a simplified model of the intersatellite link, which causes an interruption of the data transmission if the spacecraft separation exceeds a user-defined threshold.

The modeled TSX and TDX navigation solutions out of the GNSS receivers are multiplexed together with the telecommands coming from the ground segment and sent via a local network using the TCP/IP protocol to the target computer on which the flying software is running. The target computer comprises a fault-tolerant LEON-3 processor [30] implemented on a field-programmable gate array. This SPARC processor is clocked at 24 MHz and is complemented by a hard floating point unit. All RAM blocks (cache and register-file memory) are single-event-upset protected. The flight software is running in a Real-Time Executive for Multiprocessor Systems environment [31]. The relative orbit control maneuvers are multiplexed with the telemetry data and sent back to the host computer. The telemetry data are used to assess the relative navigation and control performances of the embedded system. The maneuver commands issued by TAFF as well as the absolute orbit control maneuver commands sent by the ground segment are then processed by thruster models. The thruster model converts an impulsive maneuver command to a thrust over a burn duration. The size and direction of the thrust as well as the burn duration are computed using the thruster characteristics and applying random performance and thrust direction errors. The realistic thrusts generated by the thruster model are finally sent back to the orbit propagators to be integrated over the burn duration.

A 10-day simulation based on a realistic TanDEM-X formation scenario was run. The formation was set with the following nominal configuration in meters: $(\Delta a, a\Delta \boldsymbol{e}, a\Delta \boldsymbol{i}, a\Delta u) = (0, [-150, -259], [0, 500], 65)$. The spacecraft are considered to be almost identical except for a small difference of 2% in their ballistic coefficients. Absolute maneuvers of 5 cm/s are executed every 2 days simultaneously on TDX and TSX with uncorrelated random execution errors. In the simulation, the hydrazine thruster execution errors are set to 2% rms without thrust alignment errors whereas the cold gas thrusters are affected by a 2% thrust error and 1 deg direction error. Figure 7 depicts the simulation results of the in-plane control in terms of relative orbit elements with two different control periods. The vertical dashed lines represent the simultaneous execution of a ground planed maneuver on TSX and TDX. The figure shows clearly that the differential maneuver execution errors between the ground commanded maneuvers are the main source of disturbances. They induce a sudden difference in the semimajor axis that makes the satellites drift from each other. The gain of an autonomous control system is appreciable here because the formation can be corrected right after the perturbation, avoiding the linear drift of the formation. The typical sizes of autonomous maneuvers amount to about 1.5 mm/s for a control period set to 3 orbit periods (Fig. 7d) and to about 8 mm/s for a control period set to 15 orbit periods (Figs. 7h). Figure 7 shows also clearly that the adopted control strategy greatly facilitates the prediction of the location of maneuvers, which is of great interest for mission planning and operations.

Table 1 Observer performance

Error of the estimated relative orbit elements (RMS)	
Δa	0.8 m
$a\lvert\Delta \boldsymbol{e}\rvert$	1.4 m
$a\lvert\Delta \boldsymbol{i}\rvert$	1.8 m
$a\Delta u$	2.9 m

Table 2 System performance (mean error ± standard deviation)

	Radial, m	Along track, m	Cross track, m
GPS navigation	0.0 ± 13.3	0.1 ± 5.6	0.1 ± 5.1
Filtered navigation	0.0 ± 1.4	0.0 ± 3.5	0.0 ± 1.9
Relative control $N = 3$	0.4 ± 1.8	1.1 ± 12.8	——
Relative control $N = 15$	0.1 ± 4.0	30 ± 38	——

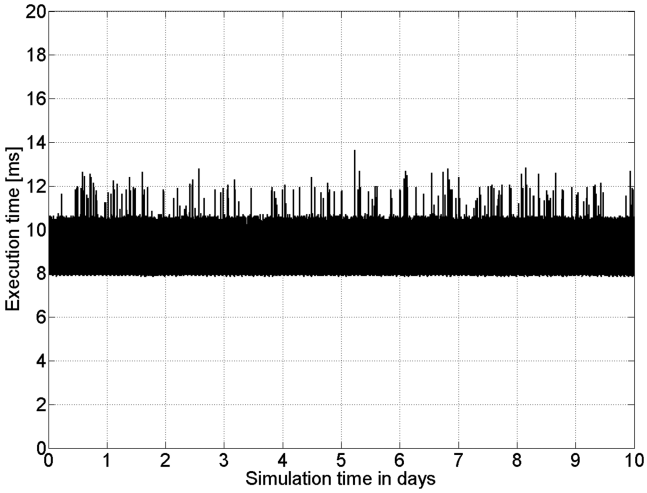

Fig. 8 Measured execution time of the TAFF component on the target computer over 10 days.

The performance of the observer is summarized in Table 1, which compares the estimated relative orbit elements of the state vector with the true relative orbit elements of the simulated formation. Overall, the observer performance is at the meter level. Numerous tests show that the filter convergence is achieved within 1 orbit.

Table 2 summarizes the modeled navigation errors of the GPS receivers as well as the achieved relative navigation and control performance for a control period set to 3 and 15 orbit periods. Despite its extreme simplicity, the extended Kalman filter reduces the noise of the GPS navigation solutions by 1 order of magnitude in the radial direction. This is of relevance for the precise control of Δa. The control performances are estimated by comparing the true relative motion out of the orbit propagator with the ideal elliptic motion defined by the chosen set of nominal relative orbit elements. Overall, the relative navigation and control accuracy are at the meter level. The control tracking errors come from the relative navigation errors but also intrinsically from the adopted control scheme. A non-vanishing relative semimajor axis is indeed created between the pair of along-track maneuvers. During a period of half an orbit, this difference in terms of Δa induces a linear drift of the spacecraft, which has to be compensated for later and which directly drives the size of the tolerance window around the mean argument of latitude (cf. Fig. 3). Table 2 shows clearly how a small control period gives much better results. This is not only due to the smaller size of the tolerance windows, but also to the fact that the perturbations of Δu [Eq. (35)] due to J_2 and the aerodynamic differential drag [Eq. (36)] were neglected during the design of the control law. Over 15 orbit periods, these contributions amount, respectively, to 2 and 17 m and are no longer negligible.

Thanks to the advanced algorithm optimizations, the impact on the onboard computer in terms of resource usage is very limited. The size of the onboard flight software is increased by about 20 kB when adding the TAFF component. Figure 8 depicts the measured flight software execution time of the complete TAFF algorithm running on the LEON-3 board. Overall, the complete algorithm is executed within 14 ms, which corresponds to a CPU load of 0.14%, because TAFF is called every 10 s.

IV. Conclusions

A simple and resource-sparing autonomous relative control system for dual spacecraft formations has been presented. The complete GNC system is based on a parameterization of the relative motion of two satellites flying on near-circular orbits, which provides a quick overview of the geometry of the relative trajectory as well as a simple criterion to assess the safety of the formation. The relative control system comprises an observer and a controller tailored to optimize the usage of resources. In particular, an analytical dynamical model of the J_2-pertubed relative motion, particularly suited

for onboard real-time applications, has been derived while the guidance and control laws make use of a closed-form analytical solution of the impulsive control problem.

The overall simplicity and intrinsic robustness of the relative control system is of interest for its integration into a real operational mission. The system presented in the paper in fact will be implemented in the TanDEM-X mission as part of the AOCS. Care has been taken to ease the ground operations and planning tasks by using a transparent and deterministic control scheme. Additional operational constraints are taken into account by using maneuver exclusion windows to disable the controller during dedicated periods.

Emphasis has been given in the paper to the realistic performance assessment and software resource usage analysis. To that end, a hardware-in-the-loop formation flying testbed has been used to demonstrate the compliance with the mission requirements. It comprises a powerful host computer simulating the environment, sensors, and actuators with a high level of precision and a real-time target computer representative of the spacecraft onboard computer. According to the simulation results, relative navigation and control performance at the meter level is expected. The impact of the GNC algorithms on the onboard computer is shown to be almost negligible in terms of the resource usage.

The TanDEM-X Autonomous Formation Flying system will demonstrate the advantages of routinely enforcing the autonomous in-plane relative control of a formation. In particular, it will improve the control performance, simplify the ground operations, and thus reduce the operational costs. It will also contribute to providing experience in designing and operating autonomously controlled formations, paving the way for future complex formation flying missions.

Acknowledgment

The TanDEM-X project is partly funded by the German Federal Ministry for Economics and Technology (Förderkennzeichen 50 EE 0601).

References

[1] Ollivier, M., Le Duigou, J-M., Mourard, D., Absil, O., Cassaing, F., Herwats, E., et al., "PEGASE: a DARWIN/TPF Pathfinder," *Proceedings of the International Astronomical Union*, Cambridge Univ. Press, Cambridge, England, UK, 2005, pp. 241–246. doi: 10.1017/S1743921306009380

[2] "LISA: Probing the Universe with Gravitational Waves," LISA Mission Science Office LISA-LIST-RP-436, Vol. 1, 2007, pp. 1–117.

[3] Moreira, A., et al., "TanDEM-X: A TerraSAR-X Add-On Satellite for Single-Pass SAR Interferometry," *Geoscience & Remote Sensing Symposium*, Vol. 2, Institute of Electrical and Electronics Engineers, New York, Sept. 2004, pp. 1000–1003. doi:10.1109/IGARSS.2004.1368578

[4] Tapley, B. D., Bettadpur, S., Watkins, M., and Reigber, C., "The Gravity Recovery and Climate Experiment: Mission Overview and Early Results," *Geophysical Research Letters*, Vol. 31, 2004, L09607. doi:10.1029/2004GL019920

[5] D'Amico, S., "Relative Orbital Elements as Integration Constants of the Hill's Equations," DLR, TN 05-08, Cologne, Germany, 2005.

[6] Clohessy, W. H., and Wiltshire, R. S., "Terminal Guidance System for Satellite Rendezvous," *Journal of the Aerospace Sciences*, Vol. 27, 1960, pp. 653–658.

[7] Hill, G. W., "Researches in the Lunar Theory," *American Journal of Mathematics*, Vol. 1, 1878, pp. 5–26. doi:10.2307/2369430

[8] Sabol, C., Burns, R., and McLaughlin, C. A., "Formation Flying Design and Evolution," *Journal of Spacecraft and Rockets*, Vol. 38, No. 2, 2001, pp. 270–278. doi:10.2514/2.3681

[9] Schweighart, S., and Sedwick, R., "High-Fidelity Linearized J_2 Model for Satellite Formation Flight," *Journal of Guidance, Control, and Dynamics*, Vol. 25, No. 6, 2002, pp. 1073–1080. doi:10.2514/2.4986

[10] Inalhan, G., Tillerson, M., and How, J. P., "Relative Dynamics and Control of Spacecraft Formations in Eccentric Orbits," *Journal of Guidance, Control, and Dynamics*, Vol. 25, No. 1, 2002, pp. 48–60. doi:10.2514/2.4874

[11] Gim, D., and Alfriend, K. T., "The State Transition Matrix of Relative Motion for the Perturbed Non-Circular Reference Orbit," AAS Paper 01-222, Feb. 2001.

[12] Kasdin, N. J., and Gurfil, P., "Canonical Modelling of Relative Spacecraft Motion via Epicyclic Orbital Elements," AIAA 2003-5591, 2003.

[13] Schaub, H., "Relative Orbit Geometry Through Classical Orbit Element Differences," *Journal of Guidance, Control, and Dynamics*, Vol. 27, No. 5, Sept.–Oct. 2004, pp. 839–848. doi:10.2514/1.12595

[14] Eckstein, M. C., Rajasingh, C. K., and Blumer, P., "Colocation Strategy and Collision Avoidance for the Geostationary Satellites at 19 degrees west," *International Symposium on Space Flight Dynamics*, 1989.

[15] Montenbruck, O., Kirschner, M., D'Amico, S., and Bettadpur, S., "E/I-Vector Separation for Safe Switching of the GRACE Formation," *Aerospace Science and Technology*, Vol. 10, 2006, pp. 628–635. doi:10.1016/j.ast.2006.04.001

[16] D'Amico, S., and Montenbruck, O., "Proximity Operations of Formation-Flying Spacecraft, Using an Eccentricity/Inclination Vector Separation," *Journal of Guidance, Control, and Dynamics*, Vol. 29, No. 3, May–June 2006, pp. 554–563. doi:10.2514/1.15114

[17] D'Amico, S., Gill, E., and Montenbruck, O., "Relative Orbit Control Design for the PRISMA Formation Flying Mission," AIAA Paper 2006-6067, Aug. 2006.

[18] Gill, E., and Runge, H., "Tight Formation Flying for an Along-Track SAR interferometer," *Acta Astronautica*, Vol. 55, No. 3–9, 2004, pp. 473–485. doi:10.1016/j.actaastro.2004.05.044

[19] Battin, R. H., *An Introduction to the Mathematics and Methods of Astrodynamics*, AIAA Education Series, AIAA, New York, 1987.

[20] Micheau, P., "Orbit Control Techniques for Low Earth Orbiting (LEO) Satellites," *Spaceflight Dynamics*, edited by J. P. Carrou, Cepadues-Editions, Toulouse, France, 1995.

[21] Schaub, H., and Alfriend, K. T., "Impulsive Feedback Control to Establish Specific Mean Orbit Elements of Spacecraft Formations," *Journal of Guidance, Control, and Dynamics*, Vol. 24, No. 4, 2001, pp. 739–745. doi:10.2514/2.4774

[22] Vaddi, S. S., Alfriend, K. T., Vadali, S. R., and Sengupta, P., "Formation Establishment and Reconfiguration Using Impulsive Control," *Journal of Guidance, Control, and Dynamics*, Vol. 28, No. 2, March–April 2005, pp. 262–268. doi:10.2514/1.6687

[23] Alfriend, K. T., Vaddi, S. S., and Lovell, T. A., "Formation Maintenance for Low Earth Near Circular Orbits," American Astronautical Society Paper 03-652, Aug. 2003.

[24] Vadali, S. R., Schaub, H., and Alfriend, K. T., "Initial Conditions and Fuel Optimal Control for Formation Flying of Satellites," AIAA Paper 1999-4265, July–Aug. 1999.

[25] Mittnacht, M., Gottzein, E., Hartrampf, M., Heim, J., and Krauss, P. A., "The MosaicGNSS Receiver Family, Orbit and Attitude Determination in Various Orbits," European Space Research and Technology Centre Paper 13.4, 2004.

[26] Brouwer, D., "Solution of the Problem of Artificial Satellite Theory Without Drag," *Astronomical Journal*, Vol. 64, No. 1274, 1959, p. 378. doi:10.1086/107958

[27] Kalman, R. E., and Bucy, R. S., "New Results in Linear Filtering and Prediction Theory," *Journal of Basic Engineering*, Vol. 83, 1961, pp. 95–108.

[28] David, R., "GRAFCET: A Powerful Tool for Specification of Logic Controllers," *IEEE Transactions on Control Systems Technology*, Vol. 3, No. 3, Sep. 1995, pp. 253–268. doi:10.1109/87.406973

[29] Montenbruck, O., Nortier, B., and Mostert, S., "A Miniature GPS Receiver for Precise Orbit Determination of the SUNSAT2004 Micro-Satellite," *ION National Technical Meeting*, Jan. 2004, pp. 636–642.

[30] Gaisler, J., "The LEON Processor User's Manual," Gaisler Research, Gothenburg, Sweden, 2001, pp. 235–237.

[31] Straumann, T., "Open Source Real Time Operating Systems Overview," *International Conference on Accelerator and Large Experimental Physics Control Systems*, 2001.